Biomaterials Science

ROYAL SOCIETY OF CHEMISTRY

PAPER

View Article Online
View Journal | View Issue

Cite this: *Biomater. Sci.*, 2024, **12**, 5753

Exosomes derived from mucoperiosteum Krt14$^+$Ctsk$^+$ cells promote bone regeneration by coupling enhanced osteogenesis and angiogenesis†

Rong Zhou,‡[a,b,c] Rui Huang,‡[a,b,c] Yue Xu,‡[a,b,c] Dandan Zhang,[a,b,c] Li Gu,[a,b,c] Yun Su,[a,b,c] Xirui Chen,[a,b,c] Wodong Shi,[a,b,c] Jing Sun,[a,b,c] Ping Gu,*[a,b,c] Ni Ni*[a,b,c] and Xiaoping Bi *[a,b,c]

Repair of large bone defects is a sophisticated physiological process involving the meticulous orchestration of cell activation, proliferation, and differentiation. Cellular interactions between different cell types are paramount for successful bone regeneration, making it a challenging yet fascinating area of research and clinical practice. With increasing evidence underscoring the essential role of exosomes in facilitating intercellular and cell–microenvironment communication, they have emerged as an encouraging therapeutic strategy to promote bone repair due to their non-immunogenicity, diverse sources, and potent bioactivity. In this study, we characterized a distinctive population of Krt14$^+$Ctsk$^+$ cells from the orbital mucoperiosteum. *In vitro* experiments confirmed that exosomes from Krt14$^+$Ctsk$^+$ cells dramatically boosted the capacities of human umbilical vein endothelial cells (HUVECs) to proliferate, migrate, and induce angiogenesis. Additionally, the exosomes notably elevated the expression of osteogenic markers, thereby indicating their potential to augment osteogenic capabilities. Furthermore, *in vivo* experiments utilizing a rat calvarial defect model verified that exosome-loaded sodium alginate (SA) hydrogels accelerated local vascularized bone regeneration within the defective regions. Collectively, these findings suggest that exosomes secreted by Krt14$^+$Ctsk$^+$ cells offer an innovative method to accelerate bone repair *via* coupling enhanced osteogenesis and angiogenesis, highlighting the therapeutic potential in bone repair.

Received 16th May 2024,
Accepted 26th September 2024

DOI: 10.1039/d4bm00673a

rsc.li/biomaterials-science

1. Introduction

Large bone defects arising from diseases and accidents severely affect the functional status and life quality of patients;[1] thus, rapid reconstruction of bone defects is necessary and urgent. Currently, available treatments, such as autologous bone transplantation and bioactive materials implantation, have inherent limitations including limited supply, increased infection rate, *etc.*[2,3]In the past few decades, thousands of strategies have been proposed to overcome difficulty in efficient bone regeneration, particularly the concept of bone tissue engineering.[4] Among these, one promising tactic is activating positive cellular cues during the physiological bone-repairing process. Growth factors and miRNA are typical ways to magnify bone regenerative response.[5,6] However, previous studies usually focused on several miRNA or proteins which are far away from the complex healing microenvironment.

Recently, exosomes have brought light to the comprehensive regulation of the bone repairing microenvironment. These extracellular vesicles, ranging in diameter from 30 to 200 nm, facilitate the transfer of a diverse cargo of biologically active substances, including genetic materials (DNA and RNA), proteins, lipids, and metabolic byproducts, to target cells.[7] This transfer occurs through various mechanisms, such as interactions between ligands and receptors, internalization, or direct merging of membranes, highlighting their crucial role in intercellular communication.[8] Exosomes exhibit no immunogenicity and can be easily produced in large quantities without changing their biological activity even at low temperatures for extended periods. Many kinds of cells have been

[a]*Department of Ophthalmology, Shanghai Ninth People's Hospital, Shanghai Jiao Tong University School of Medicine, Shanghai, 200011, P.R. China. E-mail: pinwormgo@126.com*
[b]*Shanghai Key Laboratory of Orbital Diseases and Ocular Oncology, Shanghai, 200011, P.R. China*
[c]*Center for Basic Medical Research and Innovation in Visual System Diseases, Ministry of Education, China*
†Electronic supplementary information (ESI) available. See DOI: https://doi.org/10.1039/d4bm00673a
‡First author.

proven to possess the capability of secreting exosomes, including bone marrow mesenchymal stem cells (BMSCs),[9] human umbilical cord mesenchymal stem cells (hucMSCs),[10] endothelial cells (ECs),[11] adipose-derived stem cells (ADSCs),[12] *etc.*[13–15] Numerous research studies have documented the application of exosomes within the domain of regenerative science, including the regeneration of bone,[16] the heart,[17] and the central nervous system.[18]

As for hard tissues, it has been reported that exosomes secreted by mesenchymal stem cells (MSCs) stimulated angiogenesis and osteogenesis. Mechanically, these exosomes with miRNA cargos activated downstream osteogenic signal pathways.[19–21] Despite this, implications of exosomes originating from different cells on tissue repair may vary due to diverse genomic or epigenomic profiles.[22] For example, exosomes from MSCs of different tissue origins are found to exert distinct effects on neurite outgrowth in neurons.[23] In terms of osteogenesis, exosomes originating from hucMSCs likely facilitate the mending of fractures *via* the Wnt signaling pathway.[21] In contrast, osteoclast-derived exosomes specifically hinder the function of osteoblasts.[24] These findings underscore the importance of considering the cell source and exosome composition when exploring their therapeutic potential. Besides, exosomes derived from both BMSCs and ADSCs facilitate osteogenesis of BMSCs, while BMSC-exosomes exhibit stronger bone regeneration capabilities.[25] This phenomenon indicated that exosomes derived from cells with osteogenic potential facilitate osteogenesis, and the extent of osteogenic facilitation varies according to the pro-osteogenic ability.

Periosteal stem cells originating from local periosteum are formed during development by mesenchymal cells and are currently demonstrated to be specifically labeled with $Mx1^+\alpha SMA^+$, Prrx1, or Ctsk,[26–28] possessing the intrinsic capability to proliferate, self-renew, and differentiate into osteogenic cells. Despite direct osteogenic differentiation, these skeletal stem/progenitor cells have been proved to secrete osteogenic factors during the bone healing procedure.[29,30] Recently, Weng and colleagues characterized a novel $Krt14^+Ctsk^+$ population of cells by establishing a maxillary sinus floor lifting (MSFL) murine model. This group of cells exhibit not only epithelial but also mesenchymal characteristics, along with the gene expression pattern of osteoprogenitors. In clinical patient samples and animal models, they revealed that $Krt14^+Ctsk^+$ cells figure strongly in bone formation induced by MSFL as well as in the natural balance of bone maintenance and renewal.[31] Although $Krt14^+Ctsk^+$ cells are proved to participate in bone repair, it is still obscure whether paracrine patterns (particularly exosomes) figure strongly in the process.

In this study, the osteogenic properties of $Krt14^+Ctsk^+$ cells were capitalized by extracting exosomes. In cell experiments, we found that these exosomes significantly enhanced angiogenic differentiation of HUVECs and osteogenic differentiation of BMSCs. Furthermore, hydrogels loaded with the exosomes were transplanted to the cranial defects of rats in *in vivo* experiments. The biocompatible hydrogels not only offered mechanical reinforcement to the defect site, but also facilitated vascularization and bone tissue growth through their porous structure.[32] We further evaluated bone formation and vasculogenesis in the defect regions to investigate the therapeutic efficacy of the exosome-loaded hydrogel *in vivo*. Imaging and histopathological results revealed that $Krt14^+Ctsk^+$ cell-derived exosomes dramatically promoted neovascularization and osseous restoration in the rat skull defect region. This approach provided us with insights into the regenerative paracrine function of $Krt14^+Ctsk^+$ cells on bone reconstruction and vascularization. Scheme 1 depicts the methodology and procedure of this research.

2. Materials and methods

2.1 Patient samples

Prior consent was gained from the Ethics Committee and the Animal Research Committee of the Ninth People's Hospital affiliated with Shanghai Jiao Tong University of Medicine (SH9H-2023-T243-1). The mucoperiosteum was collected from patients undergoing orbital fracture surgery. Based on the previously described method, the tissue was sequentially digested with dispase II (Maokang, Shanghai, China) and 0.06% collagenase I (Biosharp, Canada) for 1 h at 37 °C, after which the digested tissue was incubated in complete α-MEM medium, supplemented with 10% fetal bovine serum (FBS) (Corille, Australia) and 1% penicillin/streptomycin (P/S) (Gibco, New Zealand). About a week later, when the cell growth density reached 80% to 90%, passaging was conducted. After being passaged to P3, the cells were characterized by immunocytochemistry assay.

2.2 Cell lines and culture

hBMSCs (Oricell, Guangzhou, China) were cultured with 1% P/S plus 10% FBS (Oricell, Guangzhou, China) in basal medium (Oricell, Guangzhou, China). Endothelial cell basal medium (Sciencell, USA) was used to culture HUVECs (Zhongqiaoxinzhou, Shanghai, China), supplemented with 2.5% FBS, 1% P/S, and 1% endothelial cell growth supplement (ECGS). rBMSCs and $Krt14^+Ctsk^+$ cells were nurtured with complete α-MEM medium. All cells grew in incubators at 37 °C with 5% CO_2.

2.3 Exosome isolation and characterization

The complete α-MEM medium including FBS was substituted with an FBS-free medium when $Krt14^+Ctsk^+$ cells achieved a density when 80% to 90% of the plate area was covered by the cells. The conditioned medium collected after 48 h was centrifuged at 300*g* for 10 min, 2000*g* for 10 min, and 10 000*g* for 30 min. The upper liquid without sediment underwent ultracentrifugation at 100 000*g* for 70 min at 4 °C. Then samples containing pellets resuspended with PBS were spun for 70 min at 100 000*g* again. The pellet was reconstituted in PBS and preserved at −80 °C.

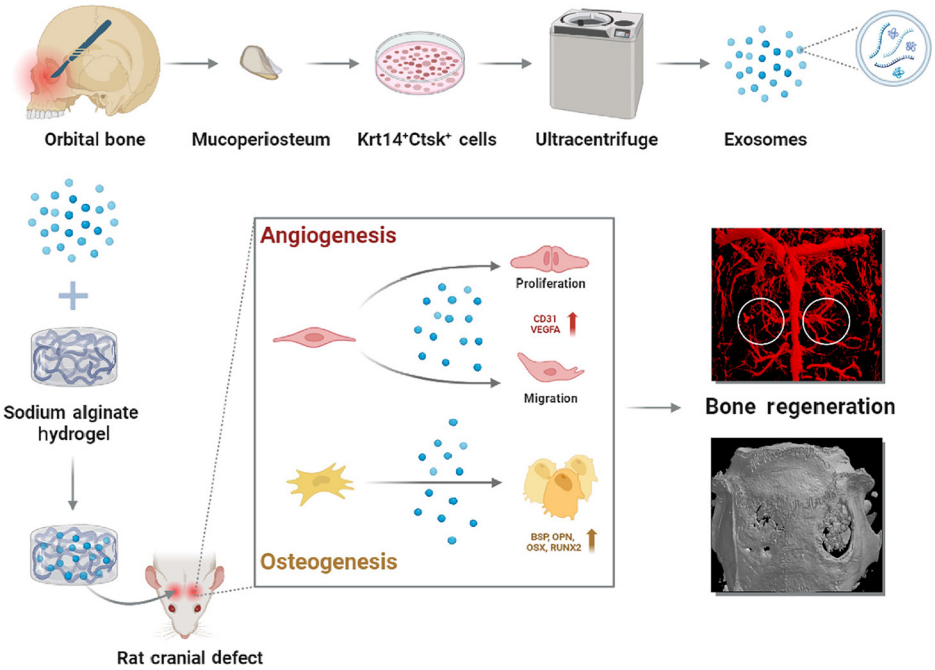

Scheme 1 The mucoperiosteum was collected and digested. Krt14^{+}Ctsk^{+} cells were grown on dishes to collect exosomes by ultracentrifuge. The exosomes capsuled with hydrogel were applied to treat rat cranial defect. In the early stage of bone healing, these exosomes promoted angiogenesis of vascular endothelial cells. Meanwhile, they stimulated osteogenic differentiation of BMSCs, accelerating osseous regeneration *in vivo*.

The size distribution of exosome particles was evaluated *via* nanoparticle tracking analysis (NTA) using Nano Sight NS300 (Malvern Panalytical, UK), while the morphology was measured by transmission electron microscope (TEM) (HT-7700, Hitachi, Japan). The exosomes were characterized by detecting exosome surface markers CD63 (1 : 1000, ab271286, UK) and TSG101 (1 : 1000, Cell Signaling Technology, USA) expression by western blot.

2.4 Cell uptake of exosomes

Diluent C was used to suspend the exosomes to 1 ml. 10 μL of PKH26 dye was added and mixed using a pipette for 30 seconds. After 5 minutes at room temperature, PKH26 was quenched by adding 10% BSA of 2 ml PBS, after which the volume was set to 8.5 ml using a serum-free medium. 0.971 M sucrose solution was prepared, and 1.5 ml sucrose solution was located to the bottom of the ultracentrifugation tube to ensure no eddy current. The liquid was centrifuged at 190 000*g* for 2 h at 2–8 °C. HUVECs or hBMSCs were cultured with exosomes labeled with PKH26 for no more than 4 hours, and the results were observed with a fluorescence microscope.

2.5 EdU assay

This experiment was performed to assess the proliferative capability of HUVECs. HUVECs during the logarithmic growth phase were planted and grew to the normal growth stage in 24-well plates. EdU solution was diluted at a 1000 : 1 ratio in cell complete medium to prepare 50 μM EdU medium. Each well was incubated with 100 μL of 50 μM EdU medium for 4 h and the medium was disposed before washing with PBS 1–2 times for 5 minutes each time. 200 μl of 4% paraformaldehyde (PFA) was placed into each well and fixed for 30 minutes, after which 200 μl of glycine 2 mg mL^{-1} was added and after incubation for 5 minutes it was washed with PBS. 500 μl of 0.5% TritonX-100 was added to each well to decolorize and incubate for 10 min, followed by washing with PBS for 5 min. At room temperature, 200 μl of Apollo reaction solution was added into each well for 30 minutes of staining. 500 μl of 0.5% Triton X-100 was added to clean 2–3 times for 10 minutes each time, and the permeation agent was discarded. After HUVECs were stained with DAPI (Thermo Fisher, USA), they were observed using a fluorescence microscope.

2.6 Scratch wound and transwell assays

Scratch wound experiments were carried out to verify the migration capability of HUVECs horizontally, while transwell assays were performed vertically. For the scratch wound assay, HUVECs underwent a scratch utilizing a pipette tip of 200 μl and were rinsed with PBS, while growing to 95% confluence in 6-well plates. The NC (control) group was supplemented with serum-free ECM plus 100 μl PBS, while the experimental group was supplemented with serum-free ECM plus exosomes. Pictures of the cells were obtained at 0 h, 12 h, and 24 h after treatment.

Transwell experiments started from seeding HUVECs into the transwell inserts placed in 24-well plates, with half FBS concentration of ECM medium plus 30 μl PBS or exosomes in inserts and normal concentration in lower wells. After 24 h of

culture, HUVECs were coagulated with 4% PFA for 15 minutes and then dyed with crystal violet for 30 minutes. The observation was performed after eliminating cells covering the top side of the inserts. ImageJ was utilized to count the number of cells on the lower surface.

2.7 Tube formation assay

150 μl Matrigel (Corning, USA) was coated onto 24-well plates at 4 °C and solidified at 37 °C for 40 min. HUVECs were seeded on Matrigel and cultured for 4–6 hours separately in ECM plus PBS or exosomes. Tube formation was photographed and analyzed with ImageJ by measuring the number of tubes, nodes and branches.

2.8 Quantitative real-time PCR

RNAs were isolated (EZBioscience, USA) and reverse transcribed to cDNA by Prime Script RT Reagent Kit (TaKaRa, Dalian, China) following the guidelines of the manufacturer. SYBR Green PCR mix (Applied Biosystems, Carlsbad, CA, USA) was implemented for qRT-PCR on LightCycler480 System (Roche, USA). ESI Table 1† displays the sequences of primers.

2.9 Western blot assay

Total protein of exosomes or cells was extracted by RIPA lysis buffer containing 1% protease inhibitor, followed by separation *via* gel electrophoresis and transfer onto PVDF membranes. The membranes were immersed in milk for 1 hour to be blocked, before being probed with primary antibodies against GAPDH (1 : 2000, ab8245, USA), RUNX2 (1 : 1000, ab236639, UK), OPN (1 : 1000, ab214050, UK), OSX (1 : 1000, ab209484, UK), BSP (1 : 1000, Cell Signaling Technology, USA), VEGFA (1 : 1000, AF5131, China), CD31 (1 : 1000, Cell Signaling Technology, USA), VEcadherin (1 : 1000, Cell Signaling Technology, USA), VEGFR2 (1 : 1000, Cell Signaling Technology, USA), TSG101 (1 : 1000, Cell Signaling Technology, USA) and CD63 (1 : 1000, ab271286, UK) overnight at 4 °C. Having been washed with TBST, the membrane was incubated with secondary antibodies conjugated to horseradish peroxidase (HRP). The protein expression level was detected with Odyssey V 3.0 image scanning (LI-COR, Lincoln, NE, USA).

2.10 Immunocytochemistry assay

Cells planted in 24-well plates were incubated with PBS and exosomes in a complete medium. Having been immobilized employing 4% PFA for 30 min, the cells were treated with PBS containing 5% goat serum for 1 h. After being incubated with primary antibodies at 4 °C for a prolonged period, cells were probed with secondary antibodies for a duration of 1 h, final staining with DAPI for 10 min was performed. Pictures of positively stained cells taken with a fluorescence microscope (Nikon) were analyzed through Image-Pro plus.

2.11 Alkaline phosphatase staining and alizarin red staining

BMSCs cultured in 6-well plates with PBS or exosomes in a complete medium for 7 days separately were fixed by 4% PFA before being stained with a BCIP/NBT alkaline phosphatase color kit (Beyotime, China).

When BMSCs grew in six-well plates for 21 days, alizarin red staining was employed to examine the influence of exosomes on the later stage of mineralization. Treated BMSCs were washed once using PBS, after which, they were immobilized with a fixative for 15 min, and washed again with PBS 3 times. Alizarin red S solution was utilized to dye for about 30 minutes. The cells with stained nodules were observed under a microscope after washing with distilled water.

2.12 Rat critical-sized calvarial defect model

All experiments involving animals were approved by the Animal Research Committee of the Ninth People's Hospital affiliated with Shanghai Jiao Tong University of Medicine (SH9H-2023-A97-1).

Anesthesia was induced in 4 week-old male Sprague-Dawley (SD) rats by injecting 50 mg kg^{-1} pentobarbital sodium intraperitoneally. A midline scalp incision of 1.5 cm was performed over the skull, followed bymeticulous scraping and removal of the periosteum, and then a symmetrical defect of the parietal bone was constructed by using a 5-mm external diameter corkscrew combined with a dental implant.[33] The hydrogel containing exosomes was then implanted in the SA + Exo group, the hydrogel alone was implanted in the SA group and nothing was implanted in the NC group, and finally the skin was sutured.

2.13 Micro-CT analysis

8 weeks after the operation, the skulls were collected and immobilized in 10% formalin. A SkyScan 1076 scanner micro-CT system (Bruker, Belgium) was employed to reconstruct the morphology of the defective area. Bone volume relative to tissue volume (BV/TV), trabecular number (Tb. N), and bone mineral density (BMD) were measured and analyzed.

2.14 Microfil perfusion

A median abdominal 10 cm sagittal incision was made after general anesthesia, fully exposing the thoracic and abdominal cavity, perfused with PBS from the aorta descendens, and perfused with Microfil (Flow Tech, MA, USA) after adequate blood flow. After being reserved at 4 °C overnight, the skulls were harvested. The collected skulls were fixed in 10% formalin and dehydrated. Finally, images of neovascularization were acquired by micro-CT.

2.15 Histological analysis

8 weeks post-surgery, the rats were euthanized, and their craniums were submerged in a 10% formalin solution prior to undergoing demineralization in EDTA for a period of 4 weeks. Following the process of fixation and demineralization, the cranial samples were encased in paraffin wax, and sections of the bone defect region were then excised and dyed with hematoxylin–eosin (HE) and Masson. Additionally, the sections were analyzed by immunohistochemical staining with CD31 and VEGFA primary antibodies.

2.16 Sequential fluorescence labeling

5 ml kg^{-1} calcein solution (Sigma, USA) and 0.8 ml kg^{-1} alizarin red (Sigma, USA) were injected intraperitoneally 2 weeks and 4 weeks after model establishment. After 8 weeks, the animals were sacrificed and the skulls were taken to make hard tissue slices. The slices were observed with a fluorescence microscope with the excitation and emission wavelengths of calcein at 488 nm and 500–550 nm, and alizarin red at 543 nm and 580–670 nm, respectively.

2.17 Statistical analysis

All statistical analyses were executed with GraphPad Prism software. The data were displayed in the format of mean ± SD, with all experiments repeated over three times. Student's *t*-tests were conducted to compare two different groups, while one-way ANOVA was applied to compare three diverse groups. Significance was inferred at $P < 0.05$, $^{*}P < 0.05$, $^{**}P < 0.01$, and $^{***}P < 0.001$.

3. Results

3.1 Paranasal sinus mucosa derived Krt14^{+}Ctsk^{+} cells secrete abundant exosomes

During MSFL surgery and bone homeostasis, a specific cluster of Krt14^{+}Ctsk^{+} cells demonstrated osteogenic potential.[31] To precisely identify and localize these cells, we conducted immunofluorescence staining on both tissue sections and isolated these cells. Immunofluorescence staining of the mucoperiosteum histological section revealed that a subset of the mucosal cells was positive for both Krt14 and Ctsk (Fig. 1A), aligning with previous reports in the literature.[31] The source of Krt14^{+}Ctsk^{+} cells was described in detail in the Materials and methods (2.1 Patient samples). Immunofluorescence staining of isolated cells also achieved a positive rate of 91.81% ± 1.13% for both markers after the cells were passaged to P3 (Fig. 1B). The cells we used for exosome extraction were all from P3 or P4. It can be assumed that the cells were Krt14^{+}Ctsk^{+} at that time.

After successfully isolating the Krt14^{+}Ctsk^{+} cell group, we proceeded with the identification of exosomes. These exosomes underwent comprehensive characterization utilizing TEM, NTA, and western blot. The images of TEM displayed cup- or round-shaped vesicles, characterized by a biconcave appearance and a double-layer membrane structure (Fig. 1C). NTA further elucidated the size distribution of the exosomes, with an average diameter at 185.3 nm (Fig. 1D). Moreover, distinctive proteins associated with exosomes, CD63 and TSG101, were validated by western blot (Fig. 1E).[34]

Subsequently, we cocultured these recipient cells with PKH26-labeled exosomes to test the endocytosis of these exosomes by BMSCs and HUVECs. Confocal microscopy images clearly demonstrated the presence of exosomes (indicated by arrows), distributed in the cytoplasm around the nucleus of both cell types (Fig. 1F). Quantitative analysis revealed that approximately 60% of the human bone marrow-derived mesenchymal stem cells (hBMSCs) and HUVECs engulfed the exosomes. These findings verified the effective isolation method of exosomes from Krt14^{+}Ctsk^{+} cells, which can be efficiently taken in by recipient cells.

3.2 The effect of Krt14^{+}Ctsk^{+} cell-derived exosomes on angiogenesis

Vascularization plays a pivotal role during bone defect repair, as angiogenesis closely correlates with bone regeneration.[35] Osteoblasts accumulate in a perivascular manner, highlighting the intimate relationship between blood vessels and bone tissue.[36] The proliferation, migration, and formation of tubular structures of vascular endothelial cells are integral to the development of blood vessels, which in turn, significantly

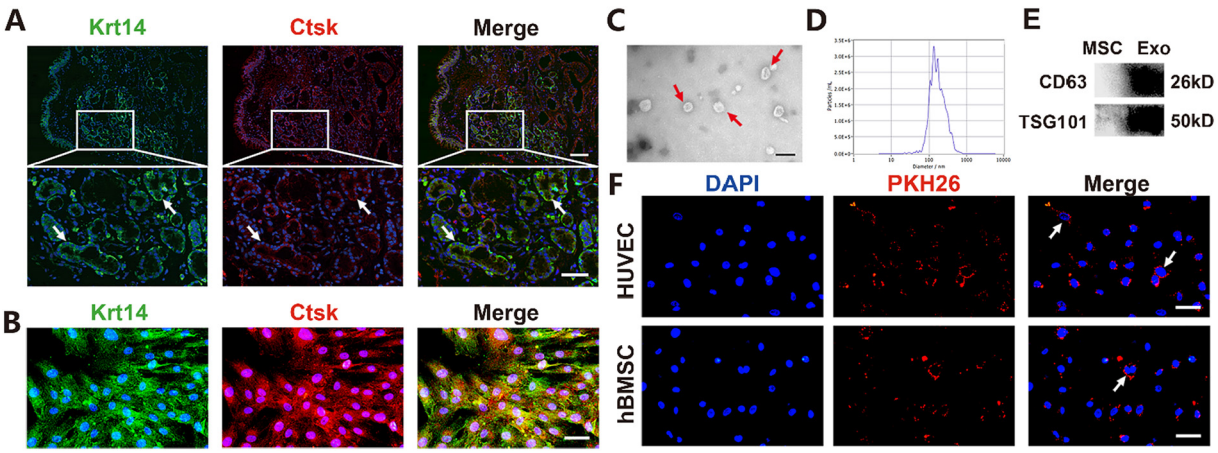

Fig. 1 Characterization of Krt14^{+}Ctsk^{+} cells and exosomes. (A) Immunofluorescence staining of mucosal tissue sections with Krt14 and Ctsk, scale bars = 100 μm. (B) Immunocytochemistry assays of cells after cultivation and passage, scale bar = 50 μm. (C) The morphology of exosomes photographed by TEM, scale bar = 100 nm. (D) The distribution of exosome particle size analyzed by NTA. (E) Western blot of the specific markers of exosomes CD63 and TSG101. (F) PKH26-labeled exosomes were phagocytosed by both HUVECs and hBMSCs, scale bars = 50 μm.

promote bone remodeling.[37] Given the established role of exosomes in stimulating vasculogenesis as reported,[38] we sought to explore the angiogenic potential of exosomes derived from Krt14$^+$Ctsk$^+$ cells. Specifically, we assessed the angiogenic response of HUVECs treated with the exosomes in the Exo group, while HUVECs in the control (NC) group were treated with PBS instead of exosomes (dissolved in PBS). To assess the proliferative capacity of HUVECs, we initially employed the EdU assay. Our findings demonstrated more positive cells in the Exo group compared to the NC group (Fig. 2A and B), which was additionally backed up by PCR analysis of ki67, the proliferation marker (Fig. 2C), which exhibited elevated mRNA expression levels in the exosome groups. Subsequently, we evaluated the migratory abilities of HUVECs using both the transwell and scratch assays, representing vertical and horizontal migration, respectively. In transwell experiments, a greater number of cells in the Exo group successfully traversed the well compared to the NC group (Fig. 2D). Similarly, in the scratch wound assay, migration areas significantly augmented in the Exo group, indicating an improvement of migratory capacity (Fig. 2E). To further investigate the proangiogenic potential of the exosomes, we conducted the tube formation

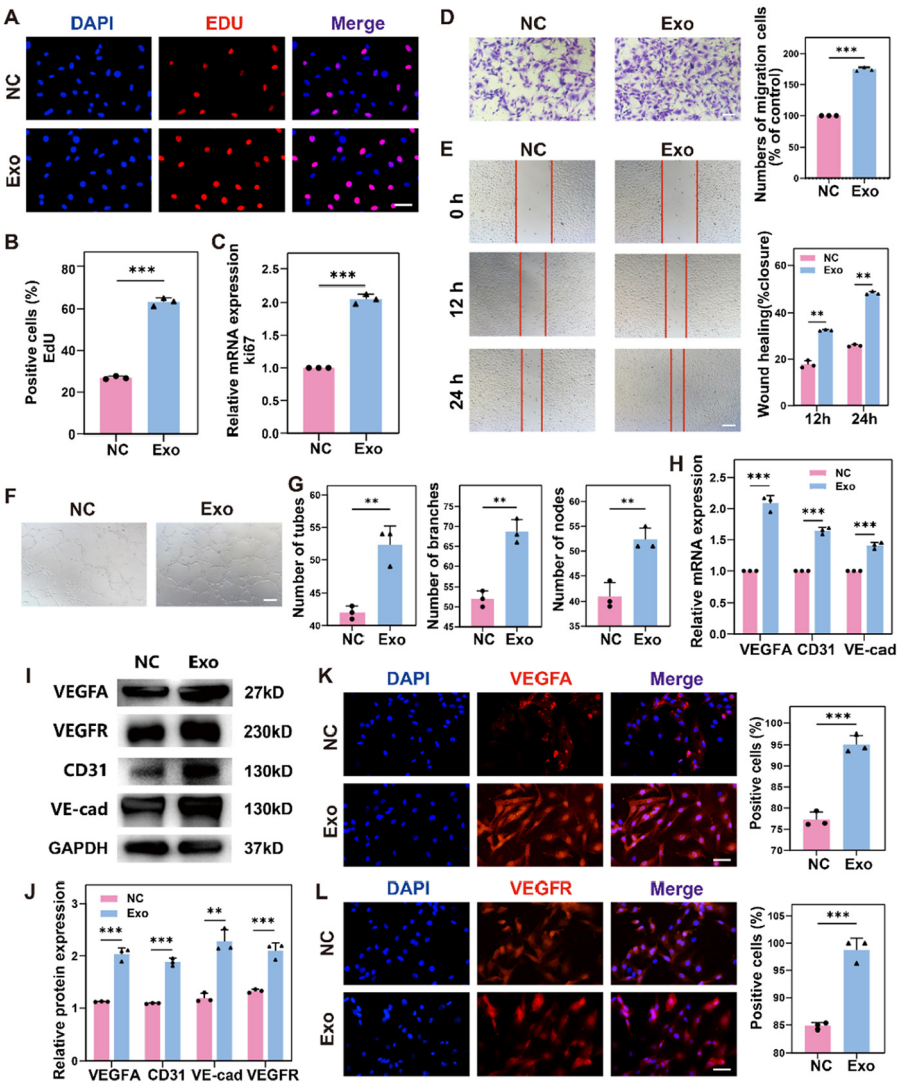

Fig. 2 The effect of Krt14$^+$Ctsk$^+$ cell-derived exosomes on the angiogenesis of HUVECs *in vitro*. (A) Photographs taken by fluorescent microscope of EdU experiments, scale bar = 50 μm. (B) The statistical analysis of the EdU assays. (C) The mRNA expression of proliferation marker ki67 of the different groups. (D) Transwell experiment: the cell migration 12 and 24 hours later, scale bar = 100 μm. (E) Scratch experiment: the cell migration at 0, 12, and 24 h after being scratched, with red lines indicating the edges of the cell migration, scale bar = 100 μm. (F) The tube formation of HUVECs 4 hours after inoculation on Matrigel, scale bar = 100 μm. (G) Statistical results of the numbers of nodes, branches, and tubes of HUVECs. (H) The mRNA expression of vascular markers (VEGFA, CD31 and VEcadherin) with or without exosome treatment. (I) The protein expression of vascular markers (VEGFA, VEGFR, CD31 and VEcadherin). (J) The statistical results of the expression of angiogenic marker proteins. (K and L) Immunocytochemistry assay to detect expression and localization of angiogenic markers VEGFA and VEGFR in the different groups, and the statistical results of the ratio of positive cells, scale bar = 50 μm. n = 3, *P < 0.05, **P < 0.01, and ***P < 0.001. The Student's t test was employed for the statistical analysis.

assay. Our results validated a notable growth in the numbers of tubes, nodes, and branches in the Exo group compared to the NC group (Fig. 2F and G). This angiogenic effect was further corroborated by the amplified mRNA expression levels of angiogenesis-related factors, containing VEGFA, CD31, and VE-cadherin (VE-cad), in the exosome groups (Fig. 2H). The analysis of western blot displayed elevated protein synthesis levels of these factors in the Exo group, along with VEGFR2, compared to the NC group (Fig. 2I and J). To provide additional evidence of the angiogenic effect of exosomes, we performed immunocytochemistry experiments. Fluorescence microscopy images clearly displayed enhanced expression of VEGFA and VEGFR2 in the Exo group compared to the NC group (Fig. 2K and L).

Taken together, these findings suggest that exosomes derived from Krt14$^+$Ctsk$^+$ cells enhance the angiogenesis of HUVECs by promoting proliferation capacity, migration ability, and tube formation, accompanied by upregulated expression of angiogenic genes.

After demonstrating the beneficial impact of exosomes on HUVEC *in vitro*, we further investigated the angiogenic potential *in vivo*. To this end, we constructed a rat model with a critical-sized skull defect, enabling us to assess the vascularization of the defect site *in vivo*. In this model, the NC group received no implantation, while the skull defects in the SA group were filled solely with SA hydrogel. The rats in the SA + Exo group were transplanted with hydrogel encapsulated with exosomes. The biosafety was verified in ESI Fig. 1.† Four weeks post-operation, during the initial phases of bone defect healing, we perfused animals with Microfil and performed microvascular CT scanning of their skulls. Our findings exhibited enhanced neovascularization in the bone defect areas treated with exosomes (Fig. 3A). Quantitative analysis further confirmed that both the number of blood vessels and the surface in the SA + Exo group obviously grew compared to the SA and NC groups (Fig. 3B). To further characterize the presence and distribution of vascular endothelial cells, we conducted an immunohistochemistry assay targeting CD31 and VEGFA markers in bone sections (Fig. 3C). The results showed elevated expression of both CD31 and VEGFA in the SA + Exo group (Fig. 3D), offering histological proof of exosome-induced neovascularization. In a word, the above results demonstrated enhanced new blood vessel formation in defect sites induced by exosomes.

Consequently, our data conclusively demonstrate that Krt14$^+$Ctsk$^+$ cell-derived exosomes figure strongly in promoting neovascularization both *in vitro* and *in vivo*, thereby presenting a favorable potential for regenerative strategies focused on vascularizing bone defects.

3.3 Krt14$^+$Ctsk$^+$ cell-derived exosomes promote osteogenic differentiation

Numerous studies have affirmed that exosomes originating from various cell types possess the capability to promote osteogenesis and angiogenesis.[39] For instance, exosomes derived from BMSCs have been found to portray resemblances in biological functionality to their parent cells.[40] Given the robust osteogenic capacity of Krt14$^+$Ctsk$^+$ cells, we hypothesized that exosomes derived from these cells were essential to osteogenic differentiation.

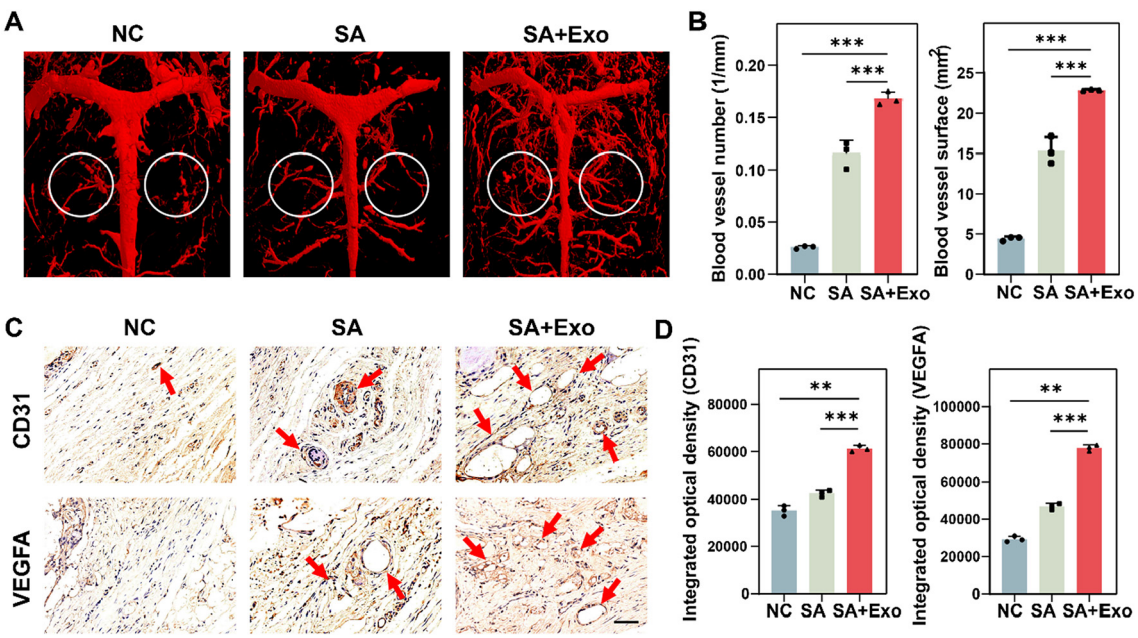

Fig. 3 The effect of Krt14$^+$Ctsk$^+$ cell-derived exosomes on the angiogenesis of HUVECs *in vivo*. (A) The results of Microfil perfusion in rat skull defect area after 4 weeks of modeling. (B) The statistical results of blood vessel surface and blood vessel numbers in the different groups. (C) The immunohistochemistry of rat skull sections, with arrows showing positive cells, scale bar = 50 μm. (D) The expression of CD31 and VEGFA in diverse groups. $n = 3$, $^*P < 0.05$, $^{**}P < 0.01$, and $^{***}P < 0.001$. The Student's t test was carried out for the statistical analysis.

To explore the osteogenic potential of exosomes secreted by Krt14$^+$Ctsk$^+$ cells, we performed ALP staining assay to detect early bone differentiation status. After seven days of osteogenic differentiation, the hBMSCs treated with exosomes exhibited pronounced staining, indicating increased ALP activity and thus, enhanced osteogenic differentiation compared to the NC group (Fig. 4A). Besides, ARS staining, a late-stage osteogenic mineralization indicator, depicted a remarkably increased number of mineralized calcium nodules in the Exo group compared with the NC group (Fig. 4B). Notably, the mRNA and protein synthesis of osteogenesis-related genes RUNX2, OSX, OPN, and BSP were notably boosted in the Exo group (Fig. 4C–

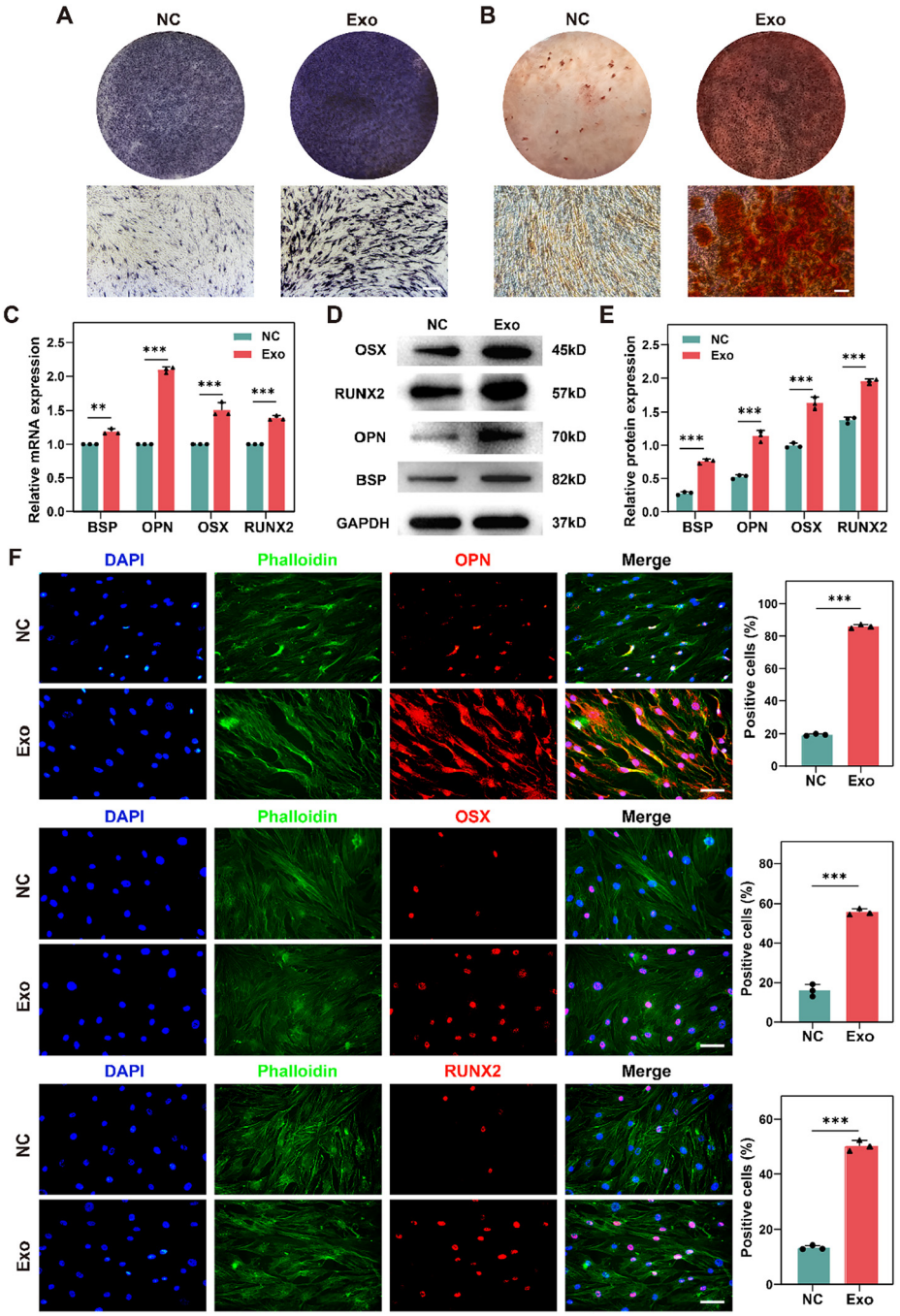

Fig. 4 The effect of Krt14$^+$Ctsk$^+$ cell-derived exosomes on osteogenic differentiation of hBMSCs. (A) Alkaline phosphatase staining, scale bar = 100 μm. (B) Alizarin red staining, scale bar = 100 μm. (C) Relative mRNA expression of osteogenic markers (BSP, OPN, OSX and RUNX2). (D) Protein expressions of osteogenic markers (BSP, OPN, OSX and RUNX2). (E) Statistical results of the expression of osteogenic marker proteins. (F) The pictures of immunocytochemistry assay depicted that the number of OPN, OSX and RUNX2 positive cells, and the statistical results of the proportion of positive cells, scale bar = 50 μm. n = 3, *P < 0.05, **P < 0.01, and ***P < 0.001. The Student's t test was applied to the statistical analysis.

E). Moreover, the immunocytochemistry (ICC) assays confirmed that hBMSCs treated with exosomes from Krt14$^+$Ctsk$^+$ cells exhibited a higher number of positive cells for osteogenic markers, including OPN, OSX, and RUNX2, compared to the NC group (Fig. 4F).

Conclusively, our findings suggest that exosomes secreted by Krt14$^+$Ctsk$^+$ cells stimulate the osteogenic differentiation of hBMSCs, providing further evidence of their potential therapeutic value in bone regeneration strategies.

After establishing the pronounced osteogenic effect of exosomes on hBMSCs, we further validated our findings in rBMSCs to justify the use of a rat model in subsequent experiments. The flow cytometry of rBMSCs is shown in ESI Fig. 2.† Similar to hBMSCs, PCR and western blot analyses proved elevated expression levels of mRNA and protein of osteogenic signature genes containing OSX, RUNX2, OPN, and BSP in rBMSCs treated with exosomes (Fig. 5A–C). Cellular-level evidence of enhanced osteogenesis was further corroborated by ICC assays, which showed a higher number of positive cells expressing osteogenic genes, including OPN, OSX, and RUNX2, in the exosome-treated groups (Fig. 5D). These experiments collectively demonstrate that exosomes significant promote rBMSC osteogenic differentiation, providing robust evidence for the feasibility and effectiveness of subsequent animal studies.

3.4 Krt14$^+$Ctsk$^+$ cell-derived exosomes accelerate bone regeneration in calvarial bone defects

We also estimated the osteogenesis of the defective bone of the animal models. 8 weeks post-surgery, the skulls of animals were either sectioned or positioned to micro-CT scanning for analysis. The results of micro-CT revealed that the skulls treated with exosomes displayed higher tissue volume (BV/TV), trabecular number (Tb. N) and bone mineral density (BMD)

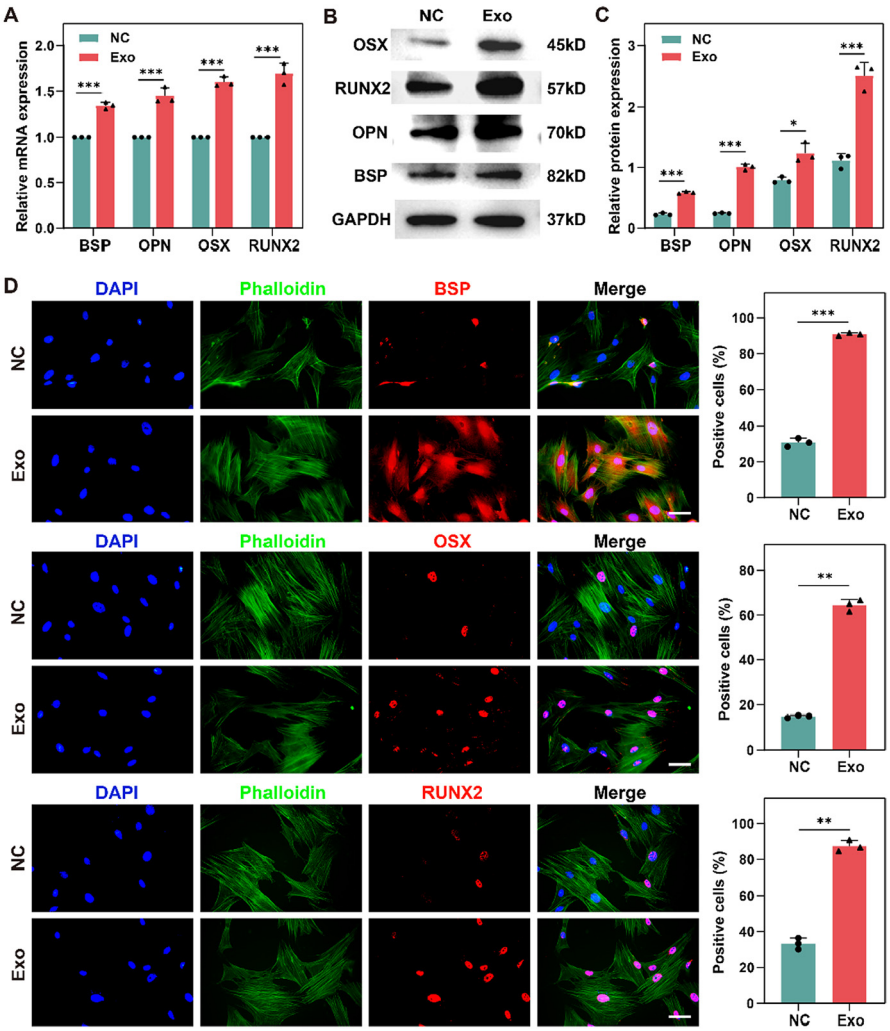

Fig. 5 The effect of Krt14$^+$Ctsk$^+$ cell-derived exosomes on the osteogenic differentiation of rBMSCs. (A) The mRNA expression of osteogenic markers (BSP, OPN, OSX and RUNX2). (B) The protein expression of osteogenic markers (BSP, OPN, OSX, and RUNX2). (C) The statistical results of the expression of osteogenic marker proteins. (D) Pictures of the immunocytochemistry assay and the statistical results of the proportion of the osteogenic markers (OPN, OSX, and RUNX2) positive cells, scale bar = 50 μm. n = 3, *P < 0.05, **P < 0.01, and ***P < 0.001. The Student's t test was utilized in the statistical analysis.

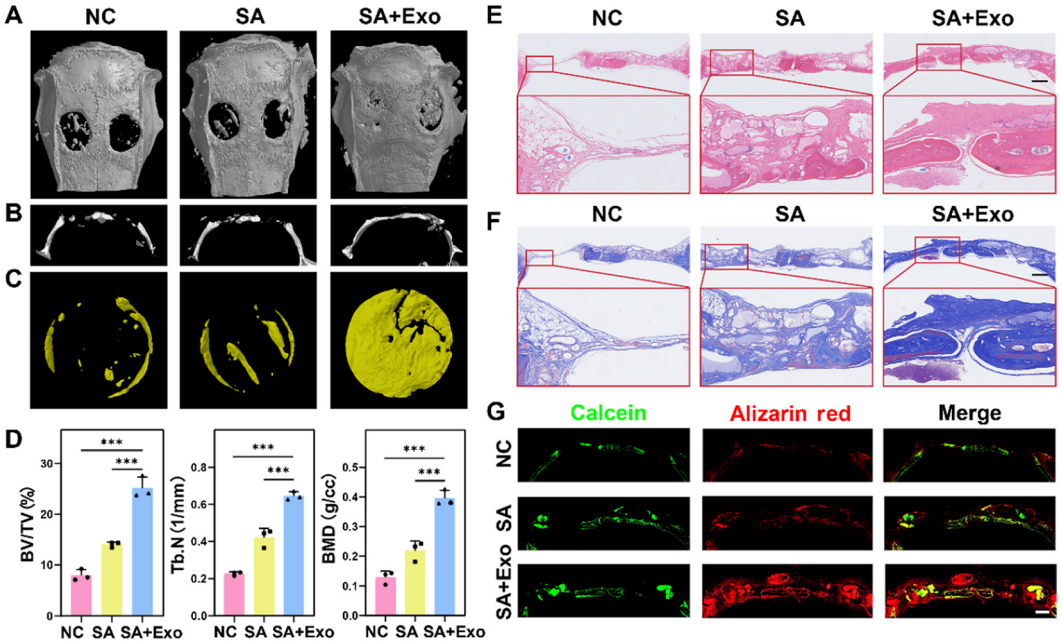

Fig. 6 The effect of Krt14$^+$Ctsk$^+$ cell-derived exosomes on rat cranial defect repair. (A) Coronal micro-CT of the rat skull defect area. (B) Sagittal micro-CT of the rat skull defect region. (C) New bone formation in the defect area of the rat skull. (D) The percent object volume, number of trabecular bones, and bone mineral density in the different groups. (E) HE staining of the defect area of the rat skull, scale bar = 1 mm. (F) Masson staining of the defect area, scale bar = 1 mm. (G) Calcein and alizarin red labeled new bone formed in the defective area of the rat skull, scale bar = 1 mm. n = 3, *P < 0.05, **P < 0.01, and ***P < 0.001. One-way ANOVA was utilized in the statistical analysis.

compared to the NC group (Fig. 6A–D). Histological staining with hematoxylin and eosin (HE) and Masson further illuminated the bone regeneration process (Fig. 6E and F). The results depicted that the regeneration of bone tissue in the SA + Exo group was most satisfactory. In the NC group, only scattered connective tissue was observed, as indicated by the arrows. The SA group fared slightly better, with the presence of both connective tissue and some nascent bone tissue alongside patches of the undergraded hydrogel. However, the SA + Exo group showed a more robust regenerative response, characterized by a significant increase in bone tissue formation, as denoted by the dark pink areas highlighted by the arrows. In addition, bone tissue sections were labeled using sequential fluorescence markers, specifically calcein and alizarin red (Fig. 6G), to identify new bone formation areas. Under fluorescence microscopy, the SA + Exo group consistently displayed a larger area of newly formed bone when compared to both the NC and SA groups. Taken together, these experimental evidence emphasize the pro-osteogenic function of Krt14$^+$Ctsk$^+$ cell-derived exosomes in facilitating bone defect repair and augmenting the regenerated bone tissue.

4. Discussion

Given the complicated anatomical characteristics and the current status of bone repair therapies, there is a pressing need to concentrate on bone tissue engineering involving *in situ* cells or cell derivatives. In our study, we extracted exosomes secreted by Krt14$^+$Ctsk$^+$ cells and demonstrated their capability to enhance neovascularization and bone regeneration, highlighting their potential as a valuable tool in regenerative medicine.

During orbital fracture repair surgery, we harvested the mucoperiosteum from the medial or inferior walls of the patients' orbits and subjected them to detailed analysis. Utilizing immunofluorescence staining, we have qualitatively and positionally identified the Krt14$^+$Ctsk$^+$ cell type, confirming their presence specifically within the mucoperiosteum covering the orbital bone. After being cultivated and passaged, over 80% of the cells tested positive for Krt14 and Ctsk. These observations were consistent with findings published by Weng *et al.*, highlighting the unique position of Krt14$^+$Ctsk$^+$ cells in bone formation triggered by MSFL and physiological stability, particularly located in the mucosa of the maxillary sinus cavity.[31] Furthermore, Liu *et al.* noted that Ctsk$^+$ cells, located in the inner lining of the orbital periosteum, exhibited notably stronger proliferative potentials in comparison to BMSCs.[41] Nevertheless, the specific contribution made by Krt14$^+$Ctsk$^+$ cells in bone repair remains elusive and needs further exploration. Numerous studies have demonstrated that intracellular interaction among osteo-lineage cells, including osteoblasts, osteoclasts, osteocytes, and MSCs, involved paracrine pathways such as the secretion of exosomes.[42,43] Specifically, exosomes derived from osteogenic cells carry essential transcription factors associated with osteogenesis, promoting osteogenic differentiation of BMSCs, the main cell sources in bone formation.[44] Thus, in our study, we extracted exosomes of

$Krt14^+Ctsk^+$ cells, characterized by TEM, NTA and protein markers, and the effect of these exosomes on HUVECs and BMSCs was systematically explored.

Generally, the vascular system plays an irreplaceable role in supporting bones with oxygen, nutrients, hormones, growth factors, neurotransmitters and stem cells. Moreover, it also removes bone metabolic products and regulates bone metabolic activity, thereby promoting bone formation, reconstruction and repair.[45] Given its significance to the skeletal system, we first assessed the angiogenic indicators to confirm the effects of exosomes originating from $Krt14^+Ctsk^+$ cells on HUVECs. The results indicated the enhanced angiogenesis of HUVECs, represented by elevated proliferative capacity, tube formation, migration ability, and expression of angiogenic factors. A multitude of investigations confirm that ECs occupy a pivotal position between blood flow and bone tissue, lining the vascular endodermis and serving a link connecting the abundant blood flow and the microenvironment of bone marrow.[46] What's more notable in our study is that the osteogenesis of both hBMSCs and rBMSCs was enhanced by exosomes, with increased expression levels of osteogenic factors. These results were consistent with the reported mechanisms of exosomes promoting osteogenesis, including recruiting stem cells, stimulating their proliferation and differentiation, inducing an osteogenic microenvironment, reducing cell senescence and apoptosis, and enhancing angiogenesis.[47,48] Exosomes represent a favorable cell-free approach for tissue regeneration, including bone, as they maintain the bioactivity of their contents over extended periods without eliciting significant immune responses in the host organism.[16] Based on our findings obtained from *in vitro* experiments, we have progressed to animal models to achieve a more thorough comprehension of the effects of exosomes *in vivo*. In these experiments, the SA hydrogel was used as the encapsulation material for exosomes given its biocompatibility, biodegradability, and rapid gelation capabilities, making it a highly versatile material for various biomedical applications.[49] In the early stage of bone repair, 4 weeks post-surgery, exosomes encapsulated in SA hydrogel at the cranial deficit area in rats significantly increased blood vessel count and surface area within the defect region. Data from micro-CT, HE and Masson staining, and sequential fluorescent labeling of defected bone sections provided evidence that exosomes effectively stimulated new bone formation *in vivo* 8 weeks after the operation. Furthermore, we also verified the biosafety of exosomes in rats, supporting their potential for therapeutic applications.

Combining *in vivo* with *in vitro* experiments, it can be concluded that exosomes stimulate the new blood vessel development in the defect area by amplifying the bioactivity of ECs to proliferate, migrate, form tubes and stimulate secretion of vascular factors. For osteogenesis, exosomes promote bone regeneration by modulating osteogenic differentiation of stem or progenitor cells. These findings may provide a plausible explanation for $Krt14^+Ctsk^+$ cells contributing to osteogenesis and physiological bone homeostasis as a coordinator. Since $Krt14^+Ctsk^+$ cells can be easily amplified, it is possible to harvest large quantities of pro-osteogenic and pro-angiogenic exosomes for bone repair. This study enhances our comprehension of the significance of mucoperiosteal progenitor cells in craniofacial bone repair, proposing a new strategy for efficient bone repair in skeletal diseases.

5. Conclusions

Briefly stated, we extracted exosomes from $Krt14^+Ctsk^+$ cells and evaluated their osteogenic efficacy. *In vitro* experiments revealed that these exosomes significantly promoted angiogenic differentiation of HUVECs and osteogenic differentiation of BMSCs. *In vivo* results also showed that exosomes enhanced angiogenesis and osteogenesis in the cranial defects of rats. Furthermore, the exosomes were incorporated into SA hydrogels, which provided mechanical reinforcement to the defect site, facilitating vascularization and bone tissue regeneration. The research demonstrated that exosomes from $Krt14^+Ctsk^+$ mucoperiosteal cells possess a remarkable ability to promote vascularization and bone regeneration. This discovery provides a new perspective on the contribution made by mucoperiosteal $Krt14^+Ctsk^+$ cells in promoting bone formation and offers a novel approach to tissue engineering for bone repair.

Ethics statement

Prior consent was gained from the Ethics Committee and the Animal Research Committee of the Ninth People's Hospital affiliated with Shanghai Jiao Tong University of Medicine (SH9H-2023-T243-1). All animal procedures were performed in accordance with the Guidelines for Care and Use of Laboratory Animals of the Ninth People's Hospital affiliated with Shanghai Jiao Tong University of Medicine and approved by the Animal Ethics Committee of the Ninth People's Hospital affiliated with Shanghai Jiao Tong University of Medicine (SH9H-2023-A97-1).

Author contributions

Conceptualization, B. X. and N. N.; methodology, H. R. and Z. D.; software, Z. R. and H. R.; validation, Z. R., X. Y., and G. L.; formal analysis, Z. R. and S. Y.; investigation, Z. R. and X. Y.; resources, S. W., S. J., and G. P.; data curation, Z. R. and C. X.; writing – original draft, Z. R.; writing – review & editing, N. N., H. R., and B. X.; visualization, Z. R.; supervision, B. X. and G. P.; project administration, B. X. and G. P.; funding acquisition, B. X.

Data availability

The authors confirm that the data supporting the findings of this study are available within the article and its ESI.†

Conflicts of interest

There are no conflicts to declare.

Acknowledgements

This work was supported by the National Natural Science Foundation of China (82171098, 82388101, 82071004, 82271123, and 82371102), Two-hundred Talent (20161419), the National Key R&D Program of China (2022YFA1105502), the Key program of Shanghai Science and Technology Commission (23JC1402400), and the Shanghai Key Clinical Specialty, Shanghai Eye Disease Research Center (2022ZZ01003).

References

1 B. C. Heng, Y. Bai, X. Li, L. W. Lim, W. Li, Z. Ge, X. Zhang and X. Deng, *Adv. Sci.*, 2023, **10**, e2204502.
2 A. Bharadwaz and A. C. Jayasuriya, *Mater. Sci. Eng., C*, 2020, **110**, 110698.
3 R. Huang, N. Ni, Y. Su, L. Gu, Y. Ju, D. Zhang, J. Li, M. Chang, Y. Chen, P. Gu and X. Fan, *Chem. Eng. J.*, 2024, **479**, 147436.
4 Z. Zhang, Z. Hao, C. Xian, Y. Fang, B. Cheng, J. Wu and J. Xia, *Acta Biomater.*, 2022, **153**, 1–12.
5 S. Sangadala, C. H. Kim, L. M. Fernandes, P. Makkar, G. R. Beck, S. D. Boden, H. Drissi and S. M. Presciutti, *eLife*, 2023, **12**, e63402.
6 L. Hu, X. Xie, H. Xue, T. Wang, A. C. Panayi, Z. Lin, Y. Xiong, F. Cao, C. Yan, L. Chen, P. Cheng, K. Zha, Y. Sun, G. Liu, C. Yu, Y. Hu, R. Tao, W. Zhou, B. Mi and G. Liu, *Exp. Mol. Med.*, 2022, **54**, 961–972.
7 J. J. Lai, Z. L. Chau, S. Y. Chen, J. J. Hill, K. V. Korpany, N. W. Liang, L. H. Lin, Y. H. Lin, J. K. Liu, Y. C. Liu, R. Lunde and W. T. Shen, *Adv. Sci.*, 2022, **9**, e2103222.
8 D. M. Pegtel and S. J. Gould, *Annu. Rev. Biochem.*, 2019, **88**, 487–514.
9 S. Liu, M. Fan, J. X. Xu, L. J. Yang, C. C. Qi, Q. R. Xia and J. F. Ge, *J. Neuroinflammation*, 2022, **19**, 35.
10 Q. Qu, L. Liu, Y. Cui, H. Liu, J. Yi, W. Bing, C. Liu, D. Jiang and Y. Bi, *Stem Cell Res. Ther.*, 2022, **13**, 352.
11 M. Yuan, K. Liu, T. Jiang, S. Li, J. Chen, Z. Wu, W. Li, R. Tan, W. Wei, X. Yang, H. Dai and Z. Chen, *J. Nanobiotechnol.*, 2022, **20**, 147.
12 T. Yuan, L. Meijia, C. Xinyao, C. Xinyue and H. Lijun, *Int. Wound J.*, 2023, **20**, 2424–2439.
13 M. Zhou, X. He, C. Mei and C. Ou, *Biomarker Res.*, 2023, **11**, 100.
14 D. Li, Y. Wang, X. Jin, D. Hu, C. Xia, H. Xu and J. Hu, *J. Neuroinflammation*, 2020, **17**, 126.
15 C. He, W. Hua, J. Liu, L. Fan, H. Wang and G. Sun, *Oncol. Lett.*, 2020, **20**, 589–600.
16 J. Wang, X. Li, S. Wang, J. Cui, X. Ren and J. Su, *Adv. Healthc. Mater.*, 2023, **12**, e2203361.
17 J. Tang, X. Cui, Z. Zhang, Y. Xu, J. Guo, B. G. Soliman, Y. Lu, Z. Qin, Q. Wang, H. Zhang, K. S. Lim, T. B. F. Woodfield and J. Zhang, *Adv. Healthc. Mater.*, 2022, **11**, e2100312.
18 L. Fan, C. Liu, X. Chen, L. Zheng, Y. Zou, H. Wen, P. Guan, F. Lu, Y. Luo, G. Tan, P. Yu, D. Chen, C. Deng, Y. Sun, L. Zhou and C. Ning, *Adv. Sci.*, 2022, **9**, e2105586.
19 L. Zhang, G. Jiao, S. Ren, X. Zhang, C. Li, W. Wu, H. Wang, H. Liu, H. Zhou and Y. Chen, *Stem Cell Res. Ther.*, 2020, **11**, 38.
20 H. Kuang, J. Ma, X. Chi, Q. Fu, Q. Zhu, W. Cao, P. Zhang and X. Xie, *ACS Appl. Mater. Interfaces*, 2023, **15**, 22805–22816.
21 J. Zhou, H. X. Liu, S. H. Li, Y. S. Gong, M. W. Zhou, J. H. Zhang and G. Y. Zhu, *Eur. Rev. Med. Pharmacol. Sci.*, 2019, **23**, 4954–4960.
22 D. G. Phinney and M. F. Pittenger, *Stem Cells*, 2017, **35**, 851–858.
23 M. A. Lopez-Verrilli, A. Caviedes, A. Cabrera, S. Sandoval, U. Wyneken and M. Khoury, *Neuroscience*, 2016, **320**, 129–139.
24 W. Sun, C. Zhao, Y. Li, L. Wang, G. Nie, J. Peng, A. Wang, P. Zhang, W. Tian, Q. Li, J. Song, C. Wang, X. Xu, Y. Tian, D. Zhao, Z. Xu, G. Zhong, B. Han, S. Ling, Y. Z. Chang and Y. Li, *Cell Discovery*, 2016, **2**, 16015.
25 A. Liu, D. Lin, H. Zhao, L. Chen, B. Cai, K. Lin and S. G. Shen, *Biomaterials*, 2021, **272**, 120718.
26 N. Zhang, L. Hu, Z. Cao, X. Liu and J. Pan, *Front. Cell Dev. Biol.*, 2022, **10**, 812094.
27 L. C. Ortinau, H. Wang, K. Lei, L. Deveza, Y. Jeong, Y. Hara, I. Grafe, S. B. Rosenfeld, D. Lee, B. Lee, D. T. Scadden and D. Park, *Cell Stem Cell*, 2019, **25**, 784–796.
28 W. Zhang, N. Wang, M. Yang, T. Sun, J. Zhang, Y. Zhao, N. Huo and Z. Li, *J. Orthop. Translat.*, 2022, **33**, 41–54.
29 O. Duchamp de Lageneste, A. Julien, R. Abou-Khalil, G. Frangi, C. Carvalho, N. Cagnard, C. Cordier, S. J. Conway and C. Colnot, *Nat. Commun.*, 2018, **9**, 773.
30 M. Chen, Y. Li, X. Huang, Y. Gu, S. Li, P. Yin, L. Zhang and P. Tang, *Bone Res.*, 2021, **9**, 21.
31 Y. Weng, H. Wang, D. Wu, S. Xu, X. Chen, J. Huang, Y. Feng, L. Li and Z. Wang, *Cell Res.*, 2022, **32**, 814–830.
32 V. P. Murali and C. A. Holmes, *Acta Biomater.*, 2021, **124**, 88–107.
33 N. Ni, M. Ge, R. Huang, D. Zhang, H. Lin, Y. Ju, Z. Tang, H. Gao, H. Zhou, Y. Chen and P. Gu, *Adv. Healthc. Mater.*, 2023, **12**, e2203107.
34 R. E. M. Qazi, Z. Sajid, C. Zhao, I. Hussain, F. Iftikhar, M. Jameel, F. U. Rehman and A. A. Mian, *Int. J. Mol. Sci.*, 2023, **24**, 10477.
35 E. J. Lee, M. Jain and S. Alimperti, *Tissue Eng., Part B*, 2021, **27**, 313–329.
36 A. N. Tikhonova, I. Dolgalev, H. Hu, K. K. Sivaraj, E. Hoxha, Á. Cuesta-Domínguez, S. Pinho, I. Akhmetzyanova, J. Gao, M. Witkowski, M. Guillamot, M. C. Gutkin, Y. Zhang, C. Marier, C. Diefenbach, S. Kousteni, A. Heguy, H. Zhong, D. R. Fooksman, J. M. Butler, A. Economides,

P. S. Frenette, R. H. Adams, R. Satija, A. Tsirigos and I. Aifantis, *Nature*, 2019, **569**, 222–228.
37 Y. Peng, S. Wu, Y. Li and J. L. Crane, *Theranostics*, 2020, **10**, 426–436.
38 Y. Zeng, X. Yao, X. Liu, X. He, L. Li, X. Liu, Z. Yan, J. Wu and B. M. Fu, *J. Extracell. Vesicles*, 2019, **8**, 1629865.
39 D. Irfan, I. Ahmad, I. Patra, R. Margiana, M. T. Rasulova, R. Sivaraman, M. Kandeel, H. J. Mohammad, Z. H. Al-Qaim, M. A. Jawad, Y. F. Mustafa and M. J. Ansari, *Cytotherapy*, 2023, **25**, 353–361.
40 X. Zhou, H. Cao, J. Guo, Y. Yuan and G. Ni, *Pharmaceutics*, 2022, **14**, 1012.
41 Z. Liu, J. Liu, J. Li, Y. Li, J. Sun, Y. Deng and H. Zhou, *Invest. Ophthalmol. Visual Sci.*, 2023, **64**, 30.
42 P. Wang, W. Shao, Z. Li, B. Wang, X. Lv, Y. Huang and Y. Feng, *Cell Commun. Signaling*, 2024, **22**, 70.
43 R. Isaac, F. C. G. Reis, W. Ying and J. M. Olefsky, *Cell Metab.*, 2021, **33**, 1744–1762.
44 K. Narayanan, S. Kumar, P. Padmanabhan, B. Gulyas, A. C. A. Wan and V. M. Rajendran, *Biomaterials*, 2018, **182**, 312–322.
45 Q. Qin, S. Lee, N. Patel, K. Walden, M. Gomez-Salazar, B. Levi and A. W. James, *Exp. Mol. Med.*, 2022, **54**, 1844–1849.
46 J. Tuckermann and R. H. Adams, *Nat. Rev. Rheumatol.*, 2021, **17**, 608–620.
47 J. Girón, N. Maurmann and P. Pranke, *J. Cell. Biochem.*, 2022, **123**, 183–201.
48 Y. Pan, Y. Li, W. Dong, B. Jiang, Y. Yu and Y. Chen, *Front. bioeng. biotechnol.*, 2023, **11**, 1167012.
49 S. Murab, A. Gupta, M. K. Włodarczyk-Biegun, A. Kumar, P. van Rijn, P. Whitlock, S. S. Han and G. Agrawal, *Carbohydr. Polym.*, 2022, **296**, 119964.